CURRENT LIMITING MECHANISMS IN ELECTRON AND ION BEAM EXPERIMENTS

R. C. Olsen

Department of Physics, Naval Postgraduate School
Monterey, California 93943–5000

Abstract. The emission and collection of current from satellites or rockets in the ionosphere is a process which, at equilibrium, requires a balance between inward and outward currents. In most active experiments in the ionosphere and magnetosphere, the emitted current exceeds the integrated thermal current by one or more orders of magnitude. The system response is typically for the emitted current to be limited by processes such as differential charging of insulating surfaces, interactions between an emitted beam and the local plasma, and interactions between the beam and local neutral gas. These current limiting mechanisms have been illustrated for 20 years in sounding rocket and satellite experiments, which are reviewed here. Detailed presentations of the SCATHA electron and ion gun experiments are used to demonstrate the general range of observed phenomena.

INTRODUCTION

The problem of exchanging large currents between a satellite and the environment is a basic one for objectives such as experiments in generating artificial aurora, operation of electrodynamic tethers, beam weapons, and active charge control. Experimental evidence accumulated over the past 20 years indicates that there may be fundamental limits on the amount of current which can be coupled to the ambient plasma, and that this current level is comparable to the thermal current which can be extracted from the ambient plasma.

The free space capacitance of a sounding rocket or satellite is quite low — typically a few hundred picofarads. Hence, currents in the mA range are sufficient to induce potentials in the kV range in milliseconds. Consequently, experiments in charge emission, such as electron beam experiments, require collection of a balancing current which is comparable to the emitted current. The thermal electron flux in the ionosphere is $J = e \, n \, \sqrt{kT_e/m_e}$ ~ 2×10^{-4} A/m^2. For a collecting area of 10 m^2, currents in the mA range are possible. An attractive potential of a few volts allows for a roughly linear increase in the collected current ($J \, \alpha \, (1+e\phi/kT)$, ignoring magnetic field effects and most sheath effects. Basic theory on such processes is addressed elsewhere in these proceedings. In principle, the potential will increase until the collected current balances the emitted current. If this potential is less than the accelerating potential for the beam, the beam escapes. It is obviously possible for this condition to be violated, if the beam energy is too low for the emitted current. (This was illustrated in ISEE–1 electron gun experiments in the magnetosphere and solar wind [Lebreton, 1983].)
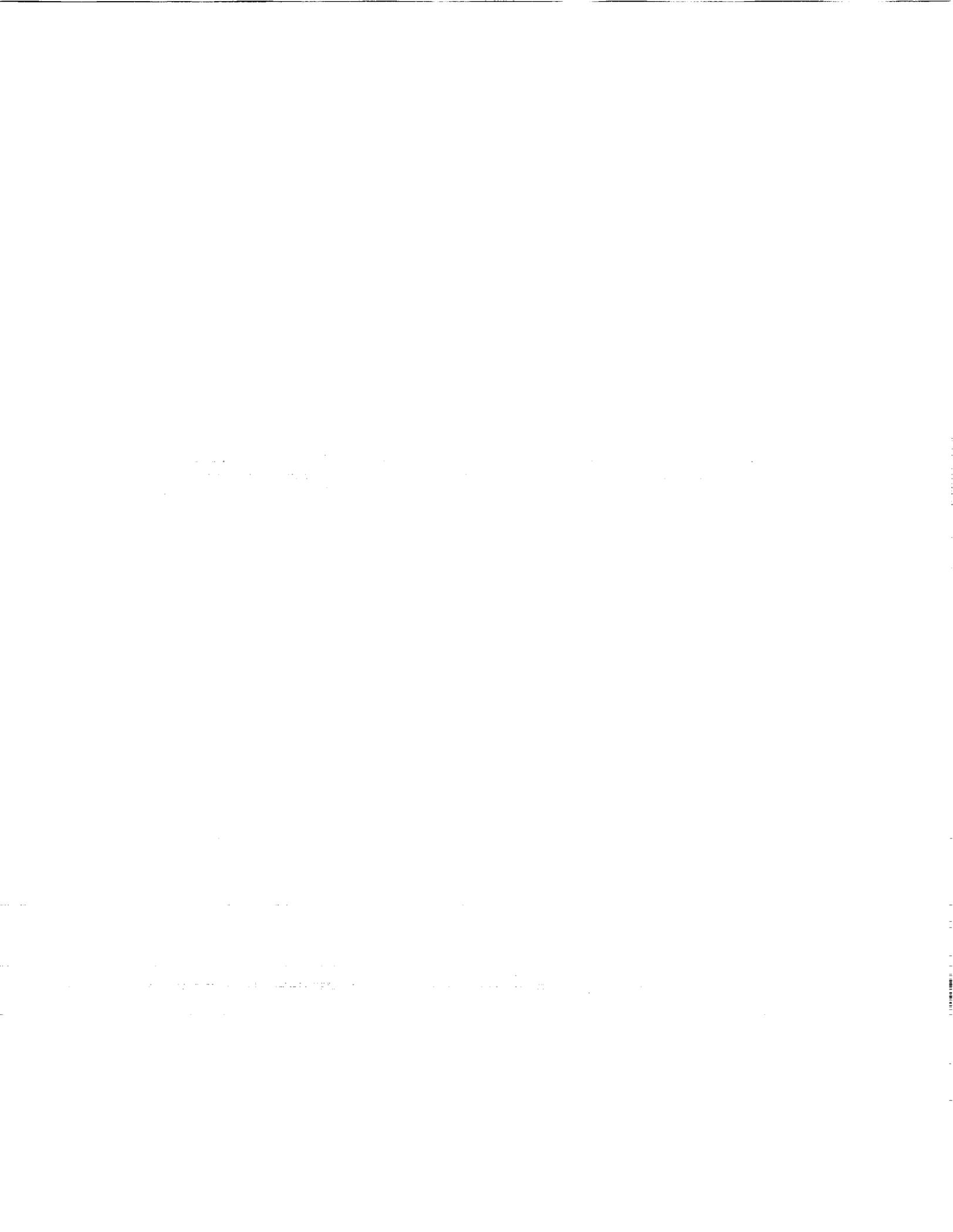
The objective of this paper is to show that in general, potentials $(q\phi)$ which are much greater than the thermal energy (kT) of the ambient plasma are not a normal solution to the current balance equation. Limiting mechanisms such as differential charging or beam–plasma interactions typically prevent the effective coupling of current from a satellite to the ambient plasma. The one caveat is that there not be a substantial neutral gas background. When neutral gas is present, nearly infinite current becomes possible.

ELECTRON BEAM EXPERIMENTS

Electron beam experiments have been conducted form sounding rockets, satellites, and the space shuttle orbiter. These experiments provide a range of environments and beam current values which span orders of magnitude in parameter space. The historical data set is considered here, with detailed presentation of recently analyzed SCATHA experiments.

SOUNDING ROCKETS

Sounding rockets experiments with electron beams have been conducted since the late 1960's, primarily with the objective of generating artificial aurora. The early experiments were conducted in the face of skepticism that kiloVolt beams could be emitted. The reasons for the skepticism were the prediction of problems with current balance (charging), and prediction that such beams would be unstable, and be disrupted by beam–plasma interactions, like the two–stream instability.

The assurance of an adequate collection of return current can be addressed by deploying a large collecting surface. For this purpose, a large inflation–deployed electron collection screen was developed and fabricated for the first US rocket–borne electron accelerator experiment. This artificial aurora experiment was launched on an Aerobie 350 from Wallops Island in January, 1969. The experiment consisted of ten electron guns capable of up to 490 mA at 9.5 keV. The rocket payload included an aluminized mylar disk, 26 m in diameter, with an inflatable hub and rim and four inflatable spokes. The collector is illustrated in Figure 1. The deployment was apparently incomplete, due to a malfunction in a pressure regulator. Nevertheless, the technique was at least partially successful. This experiment indicated that a substantial fraction of the beam current could be successfully emitted. This was shown by optical observation of artificial auroras generated by the beam at $\frac{1}{2}$A at 4.9 and 8.7 KeV, at 200 km altitude. The success eased concerns about current collection, and such extra–ordinary efforts were abandoned with most subsequent sounding rocket experiments [Hess et al, 1971].

In the ECHO series of sounding rocket experiments, electron guns with energies of 40 kV and current levels of 100 mA and above have been used to study magnetospheric plasma phenomena. Beginning with ECHO I, it was found that sufficient beam electrons propagated down to the atmosphere to generate an artificial aurora. The ECHO results were interpreted as showing that tens to hundreds of milliamps could be coupled to the ambient plasma [Winckler, 1974; 1976]. Interactions between the beam and ambient plasma were indicated by radio waves emissions particularly at the electron cyclotron frequency (f_{ce}) and harmonics. It was concluded that the beam did not lose significant power to the waves. The early ECHO experiments thereby eased concerns about the importance of beam instabilities [Cartwright and Kellogg, 1987].

The Norwegian–American experiment POLAR 5 utilized a 0.1 A, 10 keV electron beam. A "mother–daughter" pair of payloads was utilized. Diagnostics indicated charging to about 1 kV, suggesting that much of the .1 A beam escaped. Hence, sufficient return current was available at the 200 km altitude where POLAR 5 was operated to balance the beam current. It was suggested that the neutralization current was partially due to local beam–plasma interactions. The environment was unusual in that the experiment was conducted in a region with naturally occurring auroral precipitation. [Grandal et al, 1980; Jacobsen and Maynard, 1980]

The MAIMIK experiment in November 10, 1985 used an electron gun with energies of 1–3.2 kV and currents of 20–800 mA. These experiments resulted in some observations indicating that the vehicle charged to near or above beam energy, limiting the emitted current. Significant charging occurred at currents of 80 mA and above, apparently partly as a result of a low ambient plasma density ($\sim 10^4$ cm^{-3}). It appears that a virtual cathode formed outside the beam aperture, and only 1–10% of the beam escaped. The escaping electrons were accelerated to 110–120% of the beam energy [Maehlum et al, 1987; 1988].

A Soviet experiment, G–60–S, was launched in 1981, to an apogee of 1500 km (L = 2.0–2.4). The unusually high apogee allowed measurements at relatively low ambient neutral and electron densities ($n_e \approx 10^4 - 10^5/$cm^3). Only the MAIMIK experiments were conducted at comparably low plasma densities. Floating probe measurements indicated that, above 400 km altitude (n < $10^5/$cm^{-3}), the 0.5 A gun charged the vehicle to near gun energy during experiments at 1, 2 and 3 kV. Experiments at 4 kV and 5 kV caused the vehicle to charge to +6 kV and +7 kV, respectively. The 'over–charging' occurred as the gun current exceeded ~ 0.25 A. At lower currents, the vehicle potential was linearly related to gun current [Managadze et al, 1988].

The Soviet–French ARAKS experiment was one of the most ambitious experiments of the mid–1970's. ARAKS payloads were launched, on 26 January and 15 February 1975 from Kerguelen Island (L $\sim$ 3.68) to $\sim$ 200 km altitude. The 0.5 A guns operated at 15 keV and 27 keV. The guns were neutralized utilizing cesium hollow cathodes capable of 10 A plasma flux. The cathodes were apparently effective, and the electron beams apparently escaped. Vehicle potentials of a few hundred volts were inferred [Cambou et al, 1978; 1980]. VLF waves were observed, again indicating beam–plasma interactions. In particular, strong signals were observed at twice the electron gyrofrequency and at the plasma frequency. [Lavergnat et al, 1980; Dechambre et al, 1980]

These sounding rocket experiments indicate a dichotomy in results. Early experiments were interpreted as being successful in coupling currents of several hundred milliamps to the ambient, with relatively low potentials resulting. Later experiments, at higher altitudes and with better diagnostics, have been interpreted as resulting in charging of the vehicle to potentials comparable to or greater than the beam energy. These latter experiments indicate fundamental limitations on the amount of current which can be collected by a body in a plasma. The dichotomy in results may be due to differences in ambient plasma density, variations in the ionization of neutral background gas, or better instruments giving more accurate results.

SPACE SHUTTLE ORBITER

The Space Experiments with Particle Accelerator (SEPAC) was flown on the space shuttle orbiter Spacelab I payload. The Japanese–American payload was designed to generate artificial aurora using a high power electron beam. It apparently failed in this function, due to shuttle charging, and interactions between the beam and the ambient plasma and neutral gas. The charging problem was more severe than found previously on sounding rockets because of the surprisingly small conducting surface area (only the engine bells are conducting), a higher altitude (and hence lower electron density), and substantial wake effects. In particular, when the engine bells are in the wake (airplane mode flight), very little return current is available for such experiments. Interactions between the beam and local environment limited the emitted current, but may also represent a fundamental limitation in current collection [Sasaki et al, 1985, 1987; Reasoner et al, 1984; Katz et al, 1986, Marshall et al, 1988].

The electron data from these operations bear a startling similarity to SCATHA data which will be described below, and are presented here for comparison purposes. Figure 2 shows the electron flux as a function of energy during one pair of experiments. In these experiments, an argon MPD arcjet was used to generate a pulse of dense plasma, which balanced the emitted 0.3 A, 5 keV beam for ~ 10 milliseconds. The beam pulse was 5 seconds long. During the operation of the arcjet, the shuttle orbiter potential remains near plasma potential. Once the plasma generated by the MPD pulse dissipates, the vehicle charges to a potential which is estimated to be 1 kV. This inference is made by identification of the peak in the flux at 1 keV.

Converting the data to distribution function (Figure 3) shows that there is substantial plasma above and below the beam energy which must have been generated in the region of the shuttle. Even below 1 keV, there is a background plasma which apparently results from the beam operation, independent of beam neutralization. This spectrum has been interpreted as the result of space charge oscillations in the beam [Katz et al, 1986], but could be due to interactions with the neutral gas in the shuttle bay. The feature which these experiments share with the high altitude SCATHA data, presented below, is the apparent scattering of the beam, and the production of electrons at energies substantially above the beam energy.

A second (French) payload also carried on SPACELAB I was dubbed PICPAB. This lower power electron gun (10 mA, 8 kV) was designed to study wave generation. Diagnostics were inconclusive, but appear to indicate the beam operations resulted in low potentials, and hence the beam escaped. This current level is consistent with the amount of thermal electron current which is available. [Beghin et al, 1984].

SATELLITES

The ATS–5 filament neutralizer was used as an electron emitter at microampere current levels at geosynchronous orbit. ATS–5 electron emitting operations succeeded in reducing the magnitude of the negative eclipse charging potentials on the satellite. However, the spacecraft was rarely discharged

completely. This was the result of differential charging on the satellite surface limiting the emitted current [Olsen, 1985]. This is in contrast to ISEE–1 results. ISEE–1 is effectively a conducting body. Currents of 10's of microamperes were emitted, resulting in potentials up to the beam energy (~ 50 eV) [Lebreton, 1983].

SCATHA ELECTRON GUN RESULTS

The nature of the complex problems which can occur when utilizing an electron gun in space are indicated by the SCATHA results. Complex collective plasma effects occur, as well as charging effects which depend on satellite geometry and structure. SCATHA experiments were conducted with an electron gun at current levels ranging from 1 μA to 13 mA, and energies from 50 eV to 3 keV. These experiments showed that even with high energy beams differential charging or other plasma processes prevented beam emission.

DIFFERENTIAL CHARGING AS A CURRENT LIMITING MECHANISM

Data from eclipse experiments conducted with the SCATHA electron gun show how differential charging can limit electron emission. Figure 4 shows the satellite potential as a function of time for an eclipse period where the satellite charged initially to ~ −8 kV. In principle, this potential is due to an an integrated thermal electron flux in the 1–10 μA range. Even without the balancing effect of secondary electron production and the ambient ion current, it is clear that 10 μA beam current should be sufficient to discharge the satellite. The beam current and beam voltage are stepped through sequences which cover 10 μA, 100 μA and 1 mA, at 50 V and 150 V accelerating potential. The satellite potential is inferred from measurements of the ion spectrum in two detectors [Olsen, 1985]. The result is that the beam electrons result in a decrease in the magnitude of the potential, but not a complete discharge of the satellite.

This is most clearly illustrated by the 100 μA, 150 V segment at ~ 0739. The potential shows a decrease to $|\Phi|$ < 1 kV, then recharges to an equilibrium potential of ~ −1.5 kV. This curve shape, characteristic of a charging capacitor with τ ~ 1 minute, was frequently seen in the ATS–5 experiments, and indicated that the insulating solar array cover slides were charging to a potential a few hundred volts more negative than the mainframe. Equilibrium is attained when the escaping beam current has been reduced by 2 orders of magnitude. Increasing the beam current to 1 mA resulted in no increase in the escaping current. These data indicate that coupling even a low current to the ambient plasma can be difficult, due to charging phenomena. Some shuttle data also show indications of tile charging during electron beam experiments [Beghin et al, 1984].

The problems encountered in discharging a negatively charged satellite are generally unique to geosynchronous orbit. A more general class of problems became apparent during experiments in daylight and eclipse for non–charging environments. Experiments conducted when SCATHA was near plasma potential (typically a few volts positive) showed evidence of beam–plasma interactions, and a similarity to SPACELAB 1/SEPAC data which suggests the results may be quite general.

WAVE PARTICLE INTERACTIONS AS A LIMITING MECHANISM

Data from a sequence of operations on July 20, 1979 (Day 201) are presented. The example chosen here illustrates an experiment in the plasma sheet, near local midnight. July 20 was a disturbed day geomagnetically; $\Sigma Kp = 24 =$, $Kp = 2+$ for 3–6 UT. The satellite is in the plasma sheet at 0600 UT, 0130 LT, 7.4 R_E, 17° λ_m, L = 8.8. The plasma sheet electrons can be characterized with a density of 0.7 cm^{-3}, and temperature of 8.6 keV.

The data from this operation are summarized in spectrogram format in Figure 5. In a spectrogram, the instrument count rate (or particle flux) is plotted as a function of time (horizontal axis) and energy (vertical axis), with high fluxes encoded with dark gray or black, and low or zero fluxes encoded as white. The plotted value is the biased log, 1000x Log$_{10}$ (count rate +10). Hence, zero counts gives a biased log of 1000, 10^5 counts gives a biased log of 5000. Data from the two high energy detectors are shown here, with the electron data on top. The energy axis starts at zero in the middle of the figure, and increases upwards for electrons, and downwards for ions. The horizontal line plotted along the center is the pitch angle of the measured particles, which is generally near 90° at this time. Two electron gun operation periods occur during this one hour time segment (0600–0700 UT). During the first segment, the gun is turned on, and high electron fluxes are found up to 70–80 eV for the entire period. This is contrary to expectations that the peak would occur at 50 eV, as might be expected for a satellite charged to +50 V. During the second operation visible in the figure, the satellite apparently did not initially charge to the beam energy, and high fluxes of electrons are found only up to a few tens of eV. There is then a subtle change in the keV electron fluxes (a decrease) and the satellite potential apparently rises to near 50 V, and intense electron fluxes are found up to 70–80 eV. Data from the first operation are discussed next.

The electron count rate is shown for beam on conditions at 0614 UT in Figure 6. The features described in the spectrogram are apparent here. The flux peaks at 50,000 counts/sec, or a differential energy flux of $\sim 10^8$ electrons/cm^2.ster at 50–70 eV. There is not a sharp boundary at the expected potential (50V), but rather at 140% of the beam energy, 70 eV. As with the SEPAC experiment (Figure 2), there is a substantial flux above the beam energy. Further information can be obtained by converting count rate to phase space density.

The 0 − 150 eV electron data are shown as a distribution function in Figure 7. In this format (log–linear axes) Maxwellian (e.g., thermalized) distributions will appear as straight lines. When the gun is off (0609 UT), the boundary between spacecraft generated photo electrons and ambient plasma at 10 to 15 eV suggests a satellite potential of +10 to +15 V. When the gun is switched on, a different equilibrium is quickly established. SCATHA charges to near beam energy (50 eV), and enhanced fluxes appear both above and below 50 eV. There is not, however, a peak at 50 eV, as would be expected if the mono–energetic beam electrons returned to the satellite; nor is there a peak which could be attributed to cool (T$\sim$1 eV) ambient electrons which have fallen through a 50 eV potential drop. Instead, there is a local minimum at 52 eV, and a peak above 50 eV, or at least a plateau from 55 to 75 eV. Liouville's theorem requires that if the distribution functions are shifted in energy by the change in spacecraft potential ($\sim$ 35V) that they shall overlap. They do so above about 80 eV, for the unperturbed magnetospheric plasma. It is

clear from this comparison, however, that the 55 to 75 eV data represent a 'new' population, and do not simply represent a charging effect. The density in the 55 to 75 eV portion of the distribution function is about 1 cm^{-3}. This is comparable to the ambient density. The 20–45 eV electron data show a density of 124 cm^{-3}, and temperature of 6.3 eV. These latter values are appropriate for the local photo–electron cloud, heated to about twice the normal temperature.

Experiments later on this day produced similar results. Figure 8 shows electron distribution functions for 10 μa and 100 μA beam settings for operations near local dusk. The presence of a higher balancing electron flux prevents SCATHA from charging to +50 V at 10 μA, as in the latter portion of the data set shown in Figure 5 ($\sim$ 0635–0645). When the current is increased to 100 μA, the data resemble those shown in Figure 7, with a peak above 50 eV.

Observations of electron distribution functions which are symptomatic of heating suggest the need to consider the plasma wave data. Such data are available for the long electric antenna (100 m tip–to–tip) and a magnetic search coil, located 2 meters from the satellite. Data are available continuously from 8 narrowband channels which cover the 400 Hz — 100 KHz frequency range for the electric antenna, and in 4 channels from 400 Hz to 3 kHz for the magnetic antenna. Wideband data covering the range from a few hundred Hertz to 3 or 6 kHz are available for portions of each day. This latter frequency range typically includes the electron gyrofrequency, but not the plasma frequency [Koons and Cohen, 1982].

Observations associated with the second example of SCATHA electron gun experiments on 20 July 1979 (Figure 8) showed evidence of strong signals at the electron cyclotron frequency. Figure 9 shows the plasma wave data for the 4 low frequency channels of the Aerospace Corp plasma wave receiver (SC1). Data are taken from the 100 meter tip–to–tip electric field antenna, and the search coil magnetometer. The latter has proven to be sensitive to electrostatic emissions. It is apparent that substantial wave power is present. The magnetic antenna is located 2 meters from the satellite, and is therefore extremely sensitive to signals generated at the satellite. Major effects are apparent in all 4 of the magnetic channels, and a less obvious response in the electric channels. The magnetic channel saturates at 2.3 kHz for the magnetic receiver during the 10 μA beam operation. No response is seen in the electric channels at 10 kHz and above. There is a current dependence to the amplitude. Much lower amplitudes are seen in the magnetic antenna at 100 μA than at 10 μA beam current.

Figures 10 and 11 show the frequency spectra obtained from the wideband receiver before and during these experiments. The data presented here have not been widely disseminated, and are shown in some detail. The SC–1 receiver cycles between the electric and magnetic antenna every 16 seconds. The narrowband data shown in summary form in Figure 9 are expanded in Figures 10 and 11, on the same time scales as the wideband data. At this time, the wideband frequency range being plotted is 0–4 kHz, with a rolloff due to the transmission bandwidth at 3 kHz. In these displays, intense signals are plotted as black, low signals as white. The wideband receiver response is governed by an automatic gain control (AGC) which is generally driven by the most intense, monochromatic signal in the frequency range.

Figure 10 shows two aspects of the gun off data which are pertinent to the gun experiments. The wideband plot given in Figure 10a shows the existence of broad frequency range signals (0 − 2 kHz) in the electric channel which are erratic in their intensity. The narrow band channels at 400 Hz (Figure 10c) and 1.3 kHz (Figure 10b) reflect the impulsive behavior of this broad spectrum. There are interference lines in the magnetic channel at 700 Hz and 2100 Hz which are due to a tuning fork in another experiment. These lines are commonly observed in the absence of strong electro–magnetic signals.

Figure 10d shows naturally occurring electron cyclotron waves appearing intermittently, at a frequency of about 2.5 kHz. The response of the magnetic loop antenna to these electrostatic waves is not understood, but is a consistent feature of the flight instrument. Both the 3.0 kHz (Figure 10e) and 2.3 kHz (not shown) narrowband channels respond to these intense signals, as is most obvious around 82244 seconds [Koons and Edgar, 1985].

When the electron gun is switched on, a strong signal is generated at about 2.3 kHz. This is the intense signal revealed by the summary plot (Figure 9), and is the thin horizontal line in Figure 11a. The previously seen electrostatic background remains visible, and variations in the background signal are apparent in the wideband data, and the narrowband electric channels (Figure 11b, c). The magnetic loop antenna is almost saturated, though the broadness of the peak in Figure 11a is more a result of the data processing than the instrument response. These signals are very close to the electron cyclotron frequency, and we have concluded that they are most likely electron cyclotron waves. This is reinforced by Figure 11d, which shows an overlap between the naturally occurring waves found in Figure 10d with the gun generated signal.

The data illustrated in Figure 11a are typical of the period. There is a fluctuation in the frequency with spin which is not apparent in these plots. This is associated with the amplitude variation which is visible in Figure 9 in the 3 kHz magnetic channel. Study of this aspect of the data showed that it was associated with fluctuations in the solar array current with spin. Fluctuations in the solar cell currents induced changes in the local magnetic field which were 1–10 nT (1–10% of the ambient field) at the satellite surface. This places the interaction region near the beam aperture. It is tempting at this point to infer that the observed signal is scattering the beam, and heating the local electron distribution.

There is a current dependence to the induced signal, which is as might be expected. During the period illustrated in Figure 11a and 11d, the gun is set at 10 μA, 50 eV. At 82948 seconds, the gun current is increased to 100 μA. The signal at 2.5 kHz disappears, and the electric and magnetic spectra resume their unperturbed forms (Figure 11d, 11f) when the current is decreased to 10 μA at 82996 seconds, the intense signal resumes. This period corresponds to the particle data shown in Figure 8. An unfortunate aspect of this correspondence is the absence of artificially stimulated electron cyclotron waves during the 100 μA operation which results in heated electrons above 50 eV. The intense signals at 2.5–2.6 kHz are anticorrelated to the 50–70 eV peak! It may be that signals not apparent in the wideband data are responsible for the 50–70 eV electron distributions. One likely possibility would be electron plasma oscillations, or upper hybrid waves. Such waves would be well out of the wideband frequency range. There is a 10 dB increase in the 100 kHz electric

channel during both of the 100 μA beam current operations ($\sim$ 2303, 2322 UT). There are spikes in the 10 kHz data which rise 20–30 dB above background at these times, also. These would be appropriate for plasma oscillations in plasmas with densities of 100 cm^{-3} and 1 cm^{-3}, respectively. This aspect of the data is presently being studied. The electron cyclotron waves may still be responsible for the enhanced temperatures in the 0–50 eV electrons [Olsen et al, 1989].

It appears that when experiments with the electron gun exceeded the amount of current available from the ambient plasma, wave particle interactions occurred which caused the beam to scatter. Electron cyclotron waves may be the causal factor. Similar wave features were reported for the Japanese JIKIKEN (EXOS–B) satellite, with some emission stimulated at the local electron gyrofrequency by a 200 eV, 0.25–1.0 mA beam. The more common features in the JIKIKEN data were signals at twice the electron gyrofrequency, and the upper hybrid resonance frequency. [Kawashima et al, 1981; 1982]

This scattering of the beam in energy is similar to the SEPAC behavior described previously. This similarity suggests that this class of limiting mechanisms is much broader than previously suspected.

ION BEAM EXPERIMENTS

Current limiting mechanisms appear to be less severe for ion beams. The historical record primarily indicates success in propagating ion beams away from satellites and rockets.

ARCS

The Argon Release Controlled Studies (ARCS) sounding rockets used a modified form of the ion engine originally used on ECHO 1 for electron beam neutralization. Currents of $\sim$ 100 mA of Ar+ were generated at energies from 20–40 eV (ARCS–1) to $\sim$ 200 eV (ARCS–3). ARCS–1 was launched on 27 January 1980. The bulk of the beam apparently escaped. It appears that the payload charged to a potential more negative than -5V. Electrons were observed to be accelerated toward the beam emitting payload during ion beam operations. This effect was ascribed to the creation of an electric field parallel to the geomagnetic field. There also appear to have been substantial electron heating, apparently due to wave turbulence associated with beam operations.

ARCS–3 was launched on 10 February 1985 to an apogee of 406 km. This experiment showed that the injection of particles parallel or perpendicular to the geomagnetic field consistently resulted in the appearance of a population of ions at low energy ($\sim$ 15 eV) and at 90o pitch angle. These ions apparently are scattered out of the beam. Still, the bulk of the beam apparently propagated well away from the rocket, with potentials limited to $\sim$ -100 V. These experiments indicate that sounding rockets are able to draw neutralizing currents to the beam and rocket via complex processes which accelerate and thermalize the ambient plasma [Kaufmann et al, 1985; 1989; Moore et al, 1982].

PORCUPINE

The Porcupine experiments conducted by the West Germans utilized a xenon ion engine design previously utilized by the Soviet Union for their METEOR

satellites. Porcupine rockets F3 and F4 were launched in March, 1979 from the European Space Research Range to study the auroral ionosphere. The Xenon ion beam was injected perpendicular to the ambient magnetic field into the collisionless ionospheric plasma at altitudes ranging from 190 to 450 km. These experiments showed that the beam propagated nearly undistorted across the plasma. The beam was not current neutralized [Häusler et al, 1986].

ATS-4

An ion engine is a device which combines an ion beam with a charge and current balancing electron source. There is generally little net current. The first major ion engine flight experiment was ATS-4, launched on August 10, 1968. ATS-4 was intended to be a geosynchronous satellite but the booster failed to achieve a second burn. ATS-4 remained attached to its Centaur Stage booster, and remained in a low parking orbit. In spite of this failure, a number of successful ion engine tests were run. Two ion thruster systems were on board, and a spacecraft potential monitor that employed one of the gravity gradient booms as a Langmuir probe. The boom was deployed prior to the last of five ion engine test periods on ATS-4. The large ram ion currents available from the relatively dense ambient plasma precluded the achievement of appreciable neutralizer emission current except for a few brief periods (altitude 218 to 760 km, density 10 ^{10}/m^3, ambient pressure 10^{-9}-10^{-6} Torr, current 330 μA, spacecraft potential -132 V) [Hunter et al, 1969].

ATS-5

ATS-5 carried a cesium contact ion engine and filament neutralizer. The ATS-5 ion engine is shown in Figure 12. ATS-5 was launched into synchronous orbit on August 12, 1969 and stationed at 105 W longitude. Again, there was a launch failure. ATS-5 was to be gravity gradient stabilized, but ended up spinning at 100 rpm. The ion engine worked well in spite of the spin problem. Coupling potentials of less than 50 V resulted from engine operation. Induced charging experiments (no neutralization) with the ion beam in sunlight resulted in induced charging to near the beam energy. Figure 13 shows the ion count rate during one of the brief experiments. These experiments indicated the effectiveness of neutral beam emission and at least some success in emitting a non-neutral beam [Olsen, 1985].

ATS-6

ATS-6 carried twin cesium thrusters designed to test ion engine technology and their usefulness for stationkeeping on the three-axis-stabilized satellite. It was launched in 1974. ATS-6 engine operations were successful, and had the beneficial side effects of discharging the mainframe and all differentially charged surfaces. The plasma bridge neutralizer alone could also discharge large negative potentials in sunlight or eclipse. A 92 hour operation of the ion engine at 160 mA, 3 kV was successfully conducted [Olsen, 1985].

SFL

A soviet sounding rocket program dubbed an automatic ionosphere space-flight laboratory (SFL), had launches in November, 1969 and August, 1970. These experiments made use of an ion engine using surface ionization of cesium on

tungsten. The maximum value of the ion beam current was 100 mA and the effective accelerating voltage was about 2400 V. The rocket body reached −1700 V potential. The thickness of the space charge layer surrounding the SFL was inferred to be 7 m [Gavrilov, 1973].

SERT II

SERT−II (Space Electric Rocket Test II), carrying dual 15 cm diameter mercury electron bombardment ion thrusters, was launched on February 3, 1970 into a polar, sun−synchronous orbit at 1000 km altitude. The SERT II thrusters accelerated 0.25 A of Hg ions through a 3 kV potential. Hollow cathode, plasma bridge neutralizers were used. The Agena second stage was retained as part of the orbiting system [Byers, 1970].

Emissive probes flown on the SERT−II spacecraft in conjunction with the prime ion thruster experiment allowed an investigation of the interaction between the spacecraft, the ion thruster, and the ambient space plasma. One thruster operated for 5−months and the other operated for 3−months. Both thrusters failed due to sudden shorts between the high voltage grids. It was determined that the cause was sputtering of grid surfaces. They demonstrated thrust, and an absence of harmful interactions with the vehicle [Kerslake et al, 1971].

The mean SERT−II spacecraft equilibrium potential with the engine off was −6 to −8 V. This relatively high negative potential was due to the presence of exposed solar array interconnections at high positive potentials (36 Volts). With the engines on, it was possible to control the potential difference between the spacecraft and the space plasma, using the neutralizer bias. For positive bias voltages, the spacecraft was driven more negative, by an amount equal to the change in bias voltage (Figure 14). The beam to neutralizer potential remained constant (tens of volts), and the current collected by the exposed interconnects was not a factor. This was particularly true where the interconnects remained below plasma potential. When the neutralizer was biased negative with respect to the satellite, the body could be driven positive. The neutralizer to beam potential increased rapidly, and the neutralizer current increased until the device current limited. This could be explained as an increase in electron collection by the satellite [Jones et al, 1970].

SCATHA

The SCATHA satellite carried a small ion gun, capable of xenon ion currents of 300 μA, 1 mA, and 2 mA, at energies of 1 keV and 2 keV (nominal). The AFGL experiment had electron emitting filaments for beam neutralization. The SCATHA experiments indicate again the range of behavior which can be found in space, particularly the effects of collective plasma processes. Data are shown from 2 days. Day 200.

Data from operations on 19 July, 1979 (Day 200), are presented first to illustrate two modes of operation of the ion gun in sunlight. The first example of ion emission begins shortly after 2140 UT. The satellite was located in the plasmasheet near local dusk (1954−2042 LT) between L = 7.6 and 8.0 at an altitude of 7.5 R_E and a magnetic latitude of 6 degrees.

286

The particle data for this day are summarized in spectrogram format in Figure 15. In a spectrogram, instrument count rate (or particle flux) is plotted as a function of time on the horizontal axis and energy on the vertical axis. The flux magnitude is depicted using a gray scale, with high fluxes appearing a dark gray or black and low or zero fluxes showing up as light gray to white. This figure displays data from the two high–energy detectors, with the electron data on top. The energy axis is zero in the middle of the figure and increases upwards for the electrons and downwards for the ions. The lower horizontal line plot in the center is the pitch angle of the measured particles. The pitch angle is the angle between the particle's velocity vector and the magnetic field line. The upper horizontal line plot is the detector head angle. Note the plasma injection at 2149 UT, recognized by the abrupt increase in particle flux over a wide energy range. Injections are the sudden appearance of hot plasma and occur at least daily, more frequently during periods of high magnetic activity, with variable spectra [McIlwain and Whipple, 1986]. The peak in the differential electron flux (count rate) is in the 1 to 10 KeV range, typical for the plasma sheet. The upper bound on the electron flux (~10 KeV) is the result of magnetospheric convection processes and is termed the Alfven boundary. It must exceed a critical energy of 15 to 20 KeV for negative charging to occur. The high energy ion flux extends up to 80 KeV.

Unneutralized ion gun operation at 1 kV and a current setting of 1 mA begins at 2141 UT and terminates at 2301 UT. This results in satellite charging, as seen in the spectrogram as a black band representing high ion fluxes. The high fluxes are due to ambient low energy ions being accelerated into the spacecraft at the spacecraft potential energy. There are two periods of trickle mode operation (no accelerating voltage) at 2200–2203 UT and 2227–2232 UT, which correspond to the times in the spectrogram where the black ion flux band is absent. This suggests a spacecraft potential magnitude of less than 10 Volts. Analysis of the data ultimately determined that the average sunlight floating potential for this period (~ +5V) was reduced to ~ +1V by the trickle mode operation, with a net ion current of 20–50 μA emitted [Werner, 1988].

When the ion gun is activated at 2141 UT, the satellite is driven to a potential between 600 and 800 volts negative, which is significantly less than the beam energy. This is indicated in the spectrogram by a black band representing high ion fluxes. The ion flux peak is due to the ambient low energy ions being accelerated into the spacecraft at the spacecraft potential energy. Potentials of less than about ±10 Volts are difficult to determine using this method, as seen by the complete absence of any ion charging peak during the two trickle mode operations. The spacecraft potential is most accurately determined by converting flux (count rate) to the particle distribution functions. The peak at about 700 eV in the ion distribution function of Figure 16, taken at 22:10:44 UT, is interpreted to be at the spacecraft potential. Representative energy channel widths are shown using bars on the data points. Note that the energy channels overlap. An alternate potential estimate can be obtained by comparing the potential of one electric field probe to the satellite potential.

Figure 17a is a plot of the potential difference measured by the SC10 electric field experiment. A modulation at the spin period is immediately obvious. There is a turn on transient, indicating the spacecraft momentarily charges to a negative potential corresponding to the magnitude of the beam voltage. The spacecraft potential then rises (becomes less negative). This behavior is seen each time the

gun is switched on and is counter–intuitive as the beam current, plotted in Figure 17b, actually increases during the transient. Note that the beam current is measured at the beam power supply and the net beam current, which stays constant, is measured at spacecraft common.

Figure 18 shows the SC10 data at higher resolution for a period after the turn on transient. It shows the potential, with points plotted every two seconds, as measured by SC10 between 2210 UT and 2215 UT (approximately five spin periods). Also plotted in this figure is the spacecraft potential as determined by the charging peaks for the HI and LO ion detectors. Energy channel widths are shown for representative SC9 data points. The excellent agreement between the SC9 and SC10 values suggest that the SC10 experiment provides a valid measurement of the spacecraft potential during ion–emission induced charging events in sunlight. Both measurements indicate a spacecraft potential less than the beam energy. Since sufficient ion current is available to charge SCATHA to the beam energy (1 kV), there must again be a limiting factor.

Figure 19 shows a distribution function taken during ion gun operation at 22:06:28 UT. The significant feature of this figure is the second peak at an energy greater than the spacecraft potential and near the ion gun energy. This secondary peak appears to be the 1 KeV beam ions scattered into the UCSD detector. It may indicate that periodically, significant fluxes of beam ions are being returned to the satellite. The significance of this becomes more apparent after a second set of experiments is considered.

Day 47 High Voltage, HI and LO Current

Observations for 16 February, 1979 (Day 47), are presented to illustrate the effects of ion gun operation on the spacecraft in a different plasma environment using similar (Day 200) beam parameters. During initial operations of the ion gun an experimental low current mode was used. In this mode, the main discharge went out and only the keeper operated. This resulted in a beam at 1 kV and 25–50 μA. Unfortunately, the SC10 booms had not yet been deployed so electric field data are not available. These experiments were conducted in the plasmasheet at local dawn near an altitude of 5.5 R_E between L = 5.7 and 6.5. Only the results of the charging analysis are presented.

In Figure 20, the energy of the peak in the distribution function, which is close to the spacecraft potential, is plotted versus time. The turn on transient at 1449 UT again seems to show the satellite charging to near the beam energy. The potential then stabilizes near −500 Volts after one minute. This is 200 volts more positive than the Day 200 operations. Ion gun telemetry for the same period, again shows the beam current increasing during the transient. After half a minute the beam steadies at a current value near 1.05 milliamp. Note that the beam current is 50% lower than the Day 200 experiments.

At 1451 UT, the gun drops into the low current mode and a −10 to −20 Volt potential is seen for a beam current of 20–30 μA. As on Day 200 net currents in the 10 to 100 microamps range result in relatively small (Φ_{s}/c < 50V) potentials. It is apparent that 1 mA should have been sufficient to drive the vehicle to near the beam potential.

Analysis of data from other experiment periods showed that the beam rarely caused the vehicle to approach beam voltage. Increasing the beam energy from 1 to 2 kV, at 1 mA, did decrease the vehicle potential (e.g., from −900 to −1800 V on day 293, in eclipse). By contrast, varying the beam current had the opposite effect. On day 293, in eclipse, experiments at 1 kV beam energy showed that at 0.3 mA, the nominal potential was −900 V. Increasing the current to 1 mA caused the potential to rise to −800 V.

The most likely reason for this peculiar behavior is that the ion beam is space charge limited [Stannard et al, 1986]. This process is illustrated in Figure 21. Much of the beam is scattered, with some ions returning to the spacecraft at 1 keV, as seen in Figure 19. The referenced analysis was based upon simple space–charge limited diode theory and brings the predicted satellite voltages in rough agreement with experiment. Net ion beam currents of 50–60 μA were predicted to escape the near–satellite region. The reason for this behavior is the relatively small exit aperture of the SPIBS. A larger diameter beam would have been able to emit a larger net current − at least until the satellite reached beam energy.

These results, combined with reports from sounding rockets, suggest a principle similar to that indicated by the electron gun experiments. At low current levels, where sufficient ambient plasma exists to counter space charge effects and to balance the emitted current, the beams propagate freely. As the ambient density decreases, space charge limiting develops. If a neutral plasma is emitted in conjunction with the beam, the beam escapes. This is illustrated by successful ion engine experiments, and SCATHA experiments where both charge carriers were emitted.

NEUTRAL GAS

The one caveat to the principle of current limiting is that the experiment be conducted in the absence of neutral gas. The injection of a plasma or a neutral gas will neutralize a charged particle beam. The mechanisms which are important are those which result in substantial ionization of the neutral gas cloud. This may be due to the beam itself, the return (collected) electron flux, or perhaps even secondary electron emission from the vehicle surface. Under some conditions, it is believed that as the ionization process proceeds, electrostatic waves are set up, which increase the ionization rate, instigating a Beam–Plasma Discharge (BPD) [Getty and Smullin, 1963].

Neutral gas releases were tried on ECHO 1. No direct evidence of effective vehicle neutralization was obtained. Indeed, the ECHO I results have been traditionally interpreted with the thought that the rocket body provided adequate return current collection. The ECHO IV experiment again considered the effect of a neutral gas release. The 40 kV, 80 mA beam was fired through an N_2 plume. The N_2 densities were obtained by means of a photometer calibrated at 3914 Å. The return current was enhanced by the neutral N_2 and enhanced glow was found when the beam went through the N_2 cloud [Israelson and Winckler, 1979].

This technique was also used in the SEPAC experiments with a beam energy of 2.9 keV and current of 200 mA. The neutral gas plume (NGP) emitted 10^{23} molecules of nitrogen (N_2) in a 100 ms pulse. The gas release resulted in a neutral gas pressure increase in the shuttle bay, from 10^{-6} Torr to $2 − 3 \times 10^{-6}$ Torr. This

technique was apparently successful, neutralizing the beam and allowing it to escape [Marshall et al, 1988]. One curious aspect of these experiments was that the 9 keV, 10 mA PICPAB beam did not result in substantial ionization of the emitted neutrals. This may be related to the relatively low shuttle potentials induced by PICPAB (~ +10) [Burch, 1986]. There is substantial disagreement in the literature over occurrence of BPD in the SEPAC experiments [Watermann et al, 1988]

Possible occurrences of BPD during sounding rocket experiments are described by J. R. Winckler. The BPD conditions are that:

$$I = C \ V^{1.5}/B^{0.7}PL \qquad (1)$$

where V is the accelerating voltage, B the magnetic field, P the pressure and L the scale length of the experiment. Since the beam perveance is generally of the form $I\alpha V^{1.5}$, it is clear that beam perveance determines the occurrence. Winckler [1982] concludes that BPD has been observed.

SUMMARY

Analysis of existing flight data on charged particle emission indicates a general difficulty in emitting substantial current. In general, it appears that the emitted current is limited to the thermal current, or the thermal current amplified by an attractive potential which is not much larger than the plasma temperature (e.g., $e\phi/kT$ ~1). Besides current limiting, space charge limiting processes restrict the ability to emit charged particle beams. Coupling of large current to the ambient plasma requires a balancing cold plasma source which may be artificial (e.g., a gas discharge), or may be supplied by the local neutral gas environment.

ACKNOWLEDGEMENTS

REFERENCES

Beghin, C., J. P. Lebreton, B. N. Maehlum, J. Troim, P. Ingsoy, and J. L. Michau, Phenomena induced by charged particle beams, Science, 225, 188–191, 13 July1984.

Burch, J. L., Space plasma physics results from Spacelab–1, J. Space. Rockets, 23, 331–335, 1986.

Byers, D. C., and J. F. Staggs, SERT–II thruster system ground testing, J. Space. Rockets, 7, 7–14, 1970.

Cambou, F., J. Lavergnat, V. V. Migulin, A. I. Morozov, B. E. Paton, R. Pellat, A. Kh. Pyatsi, H. Rème, R. Z. Sagdeev, W. R. Sheldon, I. A. Zhulin, ARAKS – Controlled or puzzling experiment?, Nature, 271, 723–726, 23 February 1978.

Cambou, F., V. S. Dokoukine, J. Kavergnat, R. Pellat, H. Reme, A. Saint–Marc, R. Z. Sagdeev, I. A. Zhulin, General description of the ARAKS experiments, Ann. Geophys., 36, 271–283, 1980.

Cartwright, D. G., and P. J. Kellogg, Observations of radiation from an electron beam artificially injected into the ionosphere, J. Geophys. Res., 79, 1439–1457, 1974.

Dechambre, M., J. Lavergnat, R. Pellat, Waves observed by the ARAKS experiments: the VLF Range, Ann. Geophys., 36, 351–356, 1980.

Gavrilov, F. V., A. S. Myasnikov, G. G. Zhadan, G. S. Orlova, and M. V. Strokin, Some results of flight tests of an ion–engine model using surface ionization of cesium on tungsten, Kosmicheskie Issledovaniya, Vol. 11, No. 1, pp. 140–144, January–February 1973.

Getty, W. D., and L. D. Smullin, Beam–plasma discharge: buildup of oscillations, J.of Applied Physics, 34, 3421–3429, 1963.

Grandal, B., J. A. Holtet, J. Troim, B. Maehlum, and B. Pran, Observations of waves artificially stimulated by an electron beam inside a region with auroral stimulation, Planet. Space Sci., 28, 1131–1145, 1980.

Häusler, B., R. A. Treumann, O. H. Bauer, G. Haerendel, R. Bush, C. W. Carlson, B. Theile, M. C. Kelley, M. C., V. S. Dokukin, and Yu–Ya. Ruzhin, Observations of the artificially injected porcupine xenon ion beam in the ionosphere, J. Geophys. Res., 91, 287–303, 1986.

Hess, W. N., M. C. Trichel, T. N. Davis, W. C. Beggs, G. E. Kraft, E., Stassinopoulos, and E. J. Maier, Artificial aurora experiment and principle results, J. of Geophys. Res., 76, 6067–6081, 1971.

Hunter, R. E., R. O. Bartlett, R. M. Worlock, and E. L. James, Cesium contact Ion microthruster experiment aboard Applications Technology Satellite (ATS–IV), J. Space. Rockets, 6, 968–970, 1969.

Israelson, G. A., and J. R. Winckler, Effect of a neutral N_2 cloud on the electrical charging of an electron beam–emitting rocket in the ionosphere: ECHO IV, J. Geophys. Res., 84, 1442–1452, 1979.

Jacobsen, T. A. and N. C. Maynard, POLAR 5 – An electron accelerator experiment within an aurora. 3. Evidence for significant spacecraft charging by an electron accelerator at ionospheric altitudes, Planet Space Sci., 28, 291–307, 1980.

Jones, S. G., J. V. Staskus, and D. C. Byers, Preliminary Results of SERT–II Spacecraft Potential Measurements Using Hot Wire Emission Probe, NASA TM X–2083 1970.

Katz, I., G. A. Johneward, D. E. Parks, D. L. Reasoner and C. K. Purvis, Energy broadening due to spacecharge oscillations in high current electron beams, Geophys. Res. Lett., 13, 64, 1986.

Kauffman, R. L., D. N. Walker, J. C. Holmes, C. J. Pollock, R. L. Arnoldy, L. J. Cahill, and P. M. Kintner, Heavy ion beam–ionosphere interactions: Charging and neutralizing the payload, J. Geophys. Res., 94, 453–471, 1989.

Kauffmann, R. L., R. L. Arnoldy, T. E. Moore, P. M. Kintner, L. J. Cahill, Jr., and D. N. Walker, Heavy ion beam–ionosphere interactions: Electron acceleration, J. Geophys. Res., 90, 9595–9614, 1985.

Kawashima, N., and the JIKIKEN (EXOS–B) CBE Project Team, Wave Excitation in Electron Beam Experiment on Japanese Satellite "JIKIKEN (Exos–B)", in Artificial Particle Beams in Space Plasma Studies, edited by Bjorn Grandal, Plenum Press, NY, 101–110, 1982.

Kawashima, N., A. Ushikoshi, Y. Murasato, A. Morioka, H. Oya, M. Ejiri, S. Miyatake, and H. Matsumoto, Beam–plasma interaction experiment in the magnetosphere by emitting an electron beam from satellite JIKIKEN (EXOS B), J. Geomag. Geolect., 33, 145–159, 1981.

Kerslake, W. R., R. G. Goldman, and W. C. Nieberding, SERT–II Mission, thruster performance, and in–flight thrust measurements, J. Space. Rockets, 8, 213–224, 1971.

Koons, H. C. and B. C. Edgar, Observations of VLF emissions at the electron gyrofrequency, J. Geophys. Res., 90, 10961–10967, 1985.

Koons, H. C., and H. A. Cohen, Plasma Waves and Electrical Discharges Stimulated by Beam Operations on a High Altitude Satellite, in Artificial Particle Beams in Space Plasma Studies, edited by Bjorn Grandal, Plenum Press, New York, 111–120, 1982.

Lavergnat, J., M. Dechambre, R. Pellat, Yu. V. Kushnerevsky, S. A. Pullinet, Waves observed by the ARAKS experiments: Generalities, Ann. Geophys., 36, 323–332, 1980.

Lebreton, J.–P., Active control of the potential of ISEE–1 by an electron gun, Proceedings of the 17th ESLAB symposium on Spacecraft/Plasma interactions and their influence on field and particle measurements, Noordwijk, The Netherlands, 13–17 Sept 1983, ESA Sp–198, 191–197, 1983

Maehlum, B. N., J. Troim, N. C. Maynard, W. F. Denig, M. Friedrich, K. M. Torkar, Studies of the electrical charging of the tethered electron accelerator mother–daughter rocket Maimik, Geophys. Res. Lett., 15, 725–728, 1988.

Maehlum, B. N., W. F. Denig, A. A. Egeland, M. Friedrich, T. Hansen, G. K. Holmgreen, K. Maseide, N. C. Maynard, B. T. Narheim, K. Svenes, K. Torkar, J. Troim, J. D. Winningham, Maimik — A high current electron beam experiment on a sounding rocket from Andoya Rocket range, Proceedings of the 8th ESA Symposium on European Rocket and Balloon Programmes and Related Research, Sunne, Sweden, 17–23 May 1987, ESA Sp–270.

Managadze, G. G., V. M. Balebanov, A. A. Burchudladze, T. I. Gagua, N. A. Leonov, S. B. Lyakhov, A. A. Martinson, A. D. Mayorov, W. K. Riedler, M. F. Friedrich, K. M. Torkar, A. N. Laliashvili Z. Klos, and Z. Zbyszynski, Potential observations of an electron–emitting rocket payload and other related plasma measurements, Planet. Space. Sci., 36, 399–410, 1988.

Marshall, J. A., C. S. Lin, J. L. Burch, T. Obayashi, and C. Beghin, Spacelab I experiments on interactions of an energetic electron beam with neutral gas, J. Space. Rockets, 25, 361–367, 1988.

McIlwain, C. E., and E. C. Whipple, The dynamic behavior of plasmas observed near geosynchronous orbit, IEEE Trans. Plasma Sci., PS–14, 874–890, 1986.

Moore, T. E., R. L. Arnoldy, R. L. Kaufmann, L. J. Cahill, Jr., P. M. Kintner, and D. N. Walker, Anomalous auroral electron distribution due to an artificial ion beam in the ionosphere, J. Geophys. Res., 87, 7569–7579, 1982.

Olsen, R. C., Experiments in charge control of geosynchronous orbit — ATS5 and ATS6, J. Space. Rockets, 22, 254–264, 1985.

Olsen, R. C., D. R. Lowery, J. L. Roeder, Plasma wave observations during electron beam experiments at high altitudes, J. Geophys. Res., in press, 1989.

Reasoner, D. L., J. L. Burch and T. Obayashi, Analysis of electron spectra produced by SEPAC electron beams on Spacelab–1 — Evidence for strong beam plasma interactions, EOS, 65, 1042, 1984.

Sasaki, S., N. Kawashima, K. Kuriki, M. Yanagisawa, and T. Obayashi, Vehicle charging observed in SEPAC Spacelab–1 experiment, J. Space. Rockets, 23, 194–199, 1985.

Sasaki, S., N. Kawashima, K. Kuriki, M. Yanagisawa, T. Obayashi, W. T. Roberts, D. L. Reasoner, R. R. Williamson, P. M. Banks, W. W. L. Taylor, K. Akai, and J. L. Burch, Neutralization of beam–emitting spacecraft by plasma injection, J. Space. Rockets, 24, 227–231, 1987.

Stannard, P. R., I. Katz, N. Mandell, J. Cassidy, D. Parks, M. Rotenberg, P. Steen, Analysis of the charging of the SCATHA (P78–2) satellite, NASA CR–165348, S–Cubed, 1981.

Watermann, J., K. Wilhelm, K. M. Torkar, and W. Riedler, Space Shuttle Charging or beam–plasma discharge: What can electron spectrometer observations contribute to solving the question?, J. Geophys. Res., 93., 4134–4140, 1988.

Werner, P., Ion Gun Operations at High Altitudes, M.S. Thesis, Naval Postgraduate School, 1988.

Winckler, J. R., An investigation of wave particle interactions and particle dynamics using electron beams injection from sounding rockets, Space Sci. Rev., 15, 751–780, 1974.

Winckler, J. R., A Summary of Recent Results under the ECHO Program for the Study of the Magnetosphere by Artificial Electron Beams, Cosmic Physics Technical Report 168, University of Minnesota, 1 September, 1976.

Winckler, J. R., The use of artificial electron beams as probes of the distant magnetosphere, in Artificial Particle Beam in Space Plasma Studies, ed. B. Grandal, pp. 3–33, Plenum Press, New York, NY, 1982.
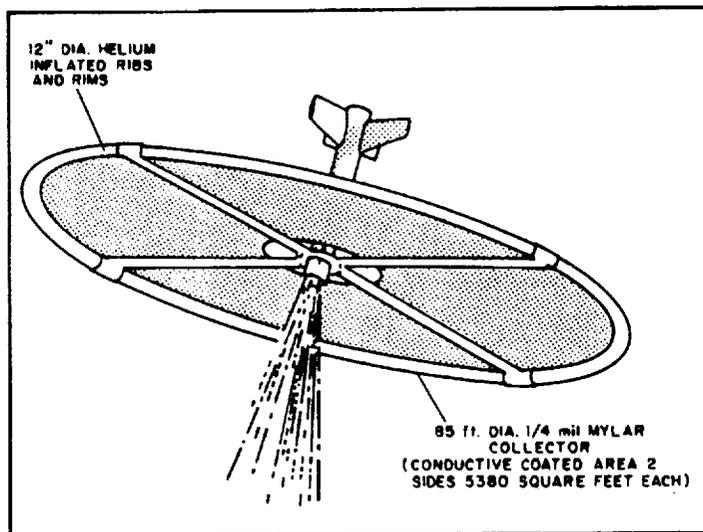
Figure 1.   Collector screen in the deployed configuration [Hess et al, 1971]
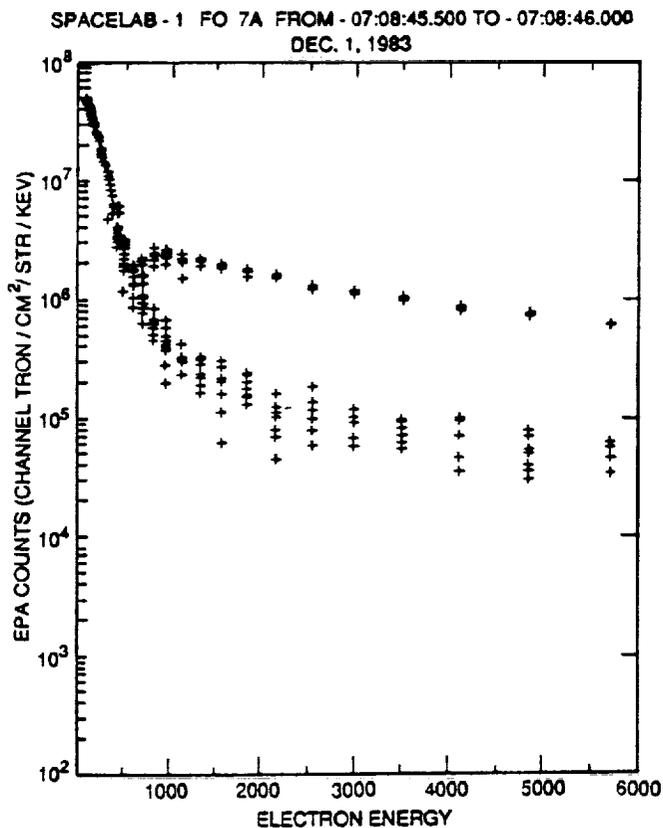
Figure 2.   SPACELAB–1/SEPAC electron differential energy flux during
electron gun firing.   Lower curve(s) are from energy sweeps
immediately after the MPD arcjet fires; upper curves follow in time
as the shuttle orbiter charges.
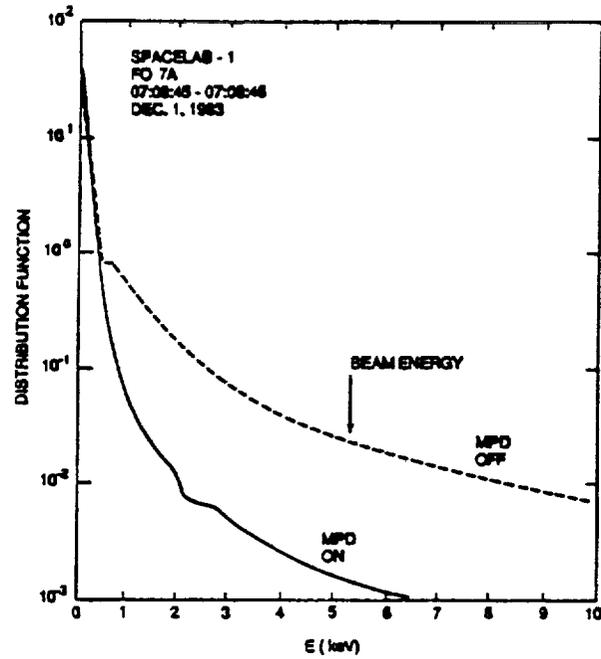
Figure 3.   SPACELAB–1/SEPAC electron distribution functions calculated
              from the data presented in Figure 2.
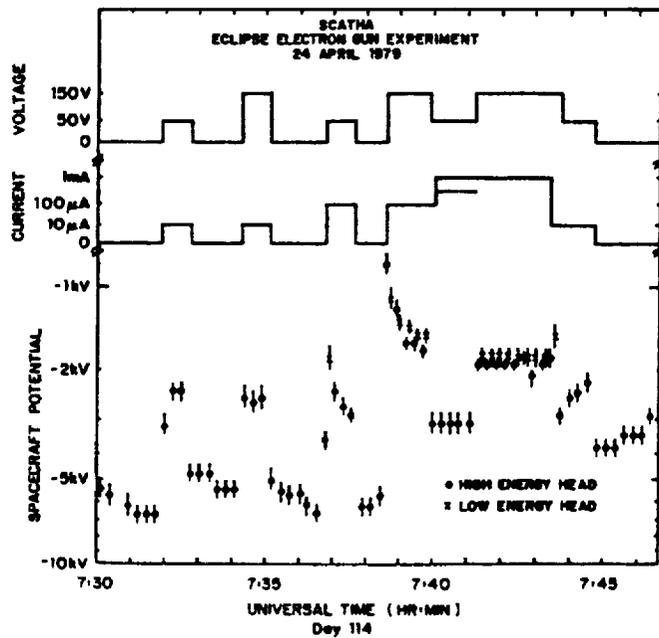
Figure 4.   SCATHA (P78–2) potential profile during eclipse gun operations on
              24 April 1979 (Day 114). Electron gun parameters are given in the
              top two plots. Spacecraft potential is estimated from the UCSD ion
              spectrometers.

SCATHA — Day 201 of 1979
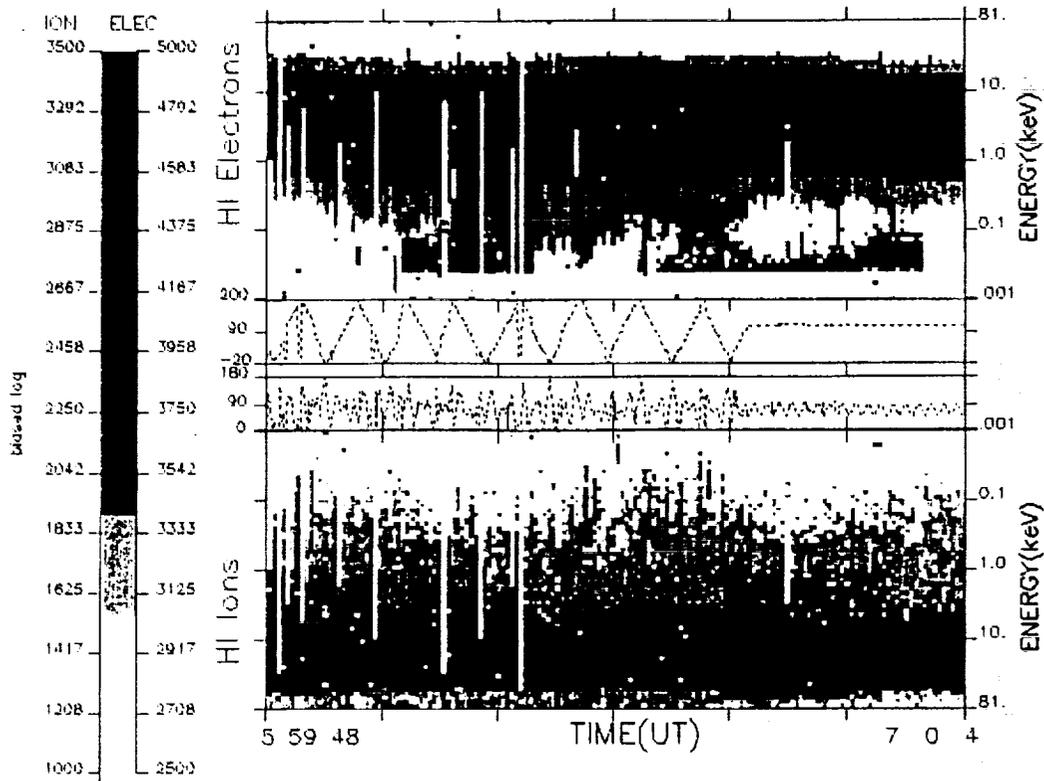
Figure 5.   SCATHA (P-78-2) electrostatic analyzer data from 20 July 1979 (Day 201) during daylight electron beam experiments.

SCATHA
20 July 1979
HI ELECTRON COUNT RATE
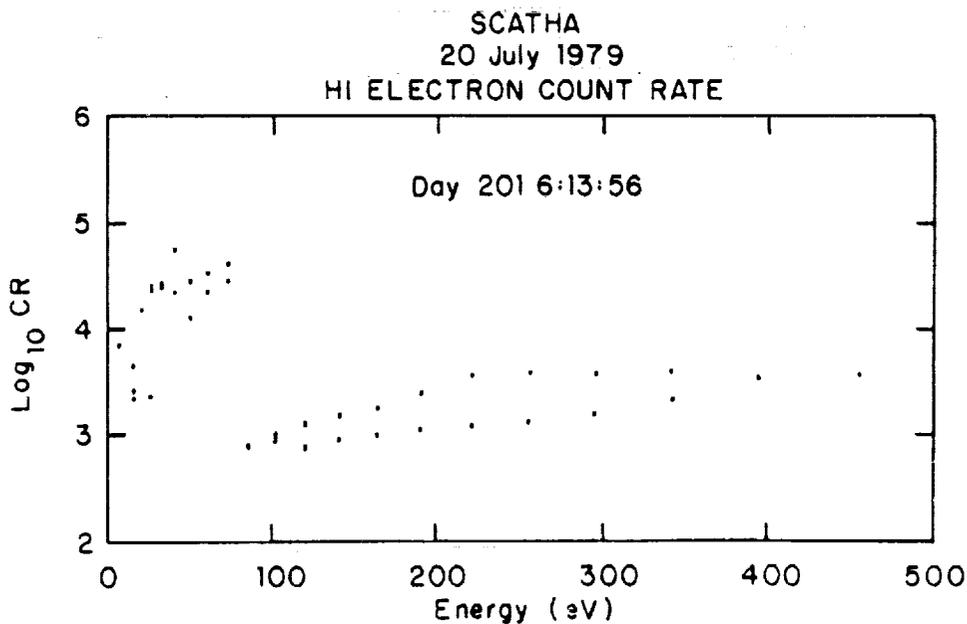
Figure 6.   SCATHA electron data during electron beam experiments. Two successive energy sweeps are shown (~ 20 seconds/sweep). For the beam on at 50 eV, 10 μA.

SCATHA
ELECTRON DISTBUTION FUNCTIONS
20 July 1979
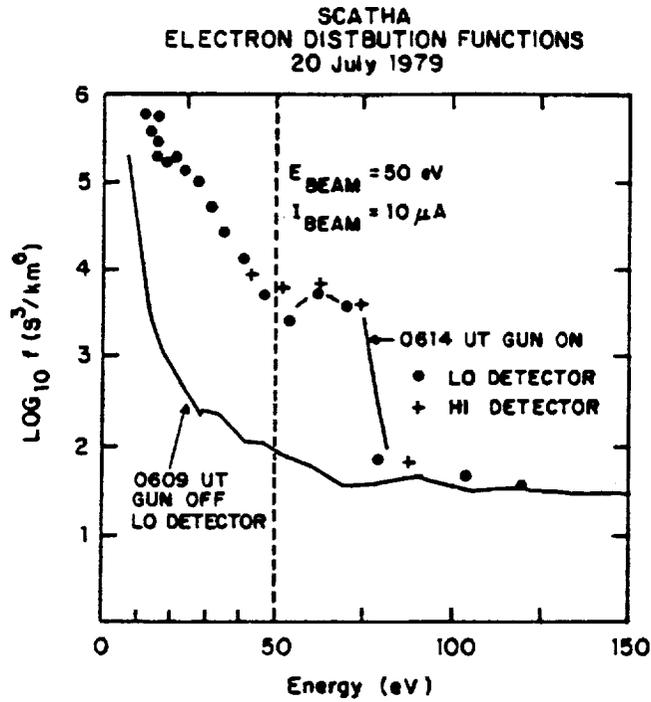
Figure 7.   SCATHA electron data from Figure 6, converted to distribution functions, and compared to gun off data (lower curve).

SCATHA
ELECTRON GUN OPERATION
DAY 201 OF 1979
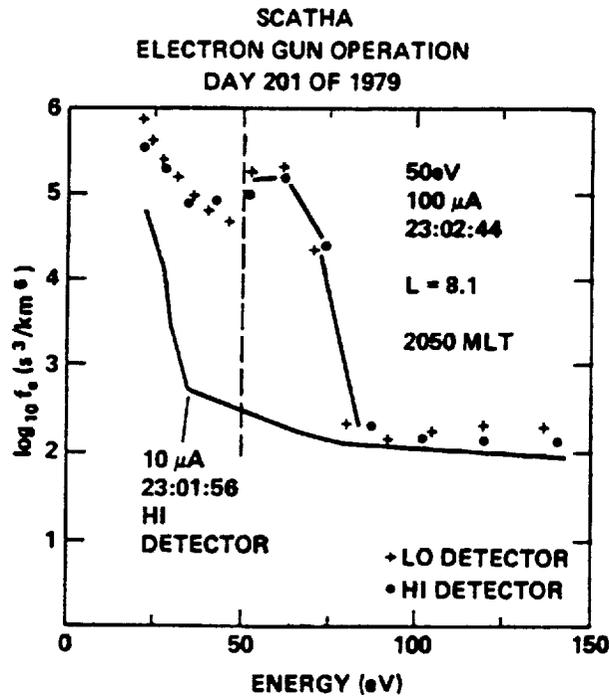
Figure 8.   SCATHA electron data, presented as distributions functions (phase space density) for electron beam operations at 50 eV, 10 μA and 100 μA.

297

SCATHA — PLASMA WAVE DATA
20 JULY 1979
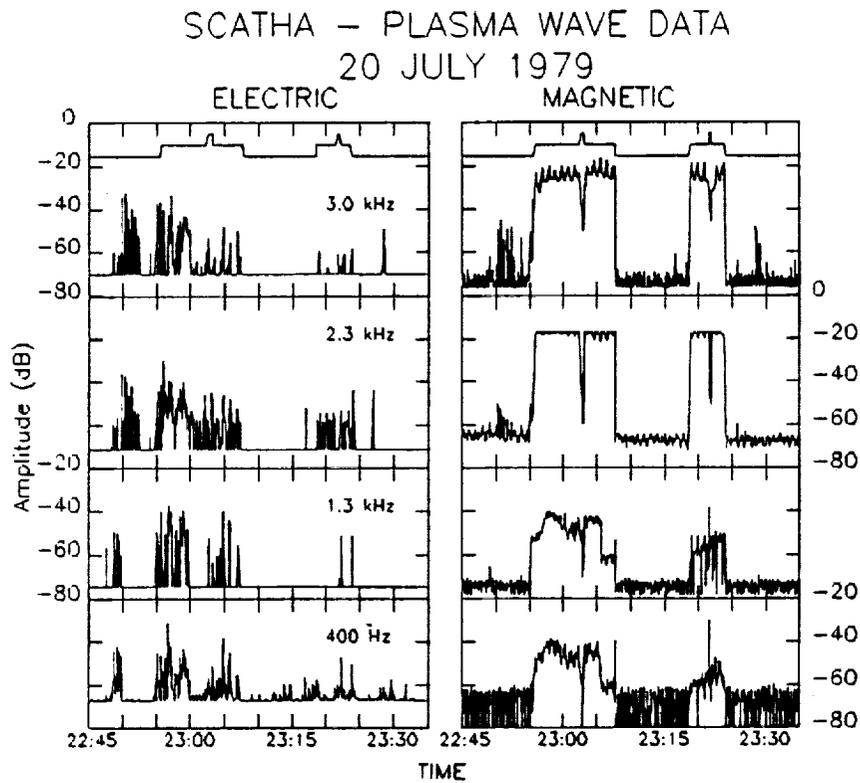
Figure 9.   SCATHA plasma wave data during electron beam experiments. The 50 eV beam is set at 0, 10 μA and 100 μA as indicated by the horizontal line in the 3.0 kHz electric and magnetic channel boxes.
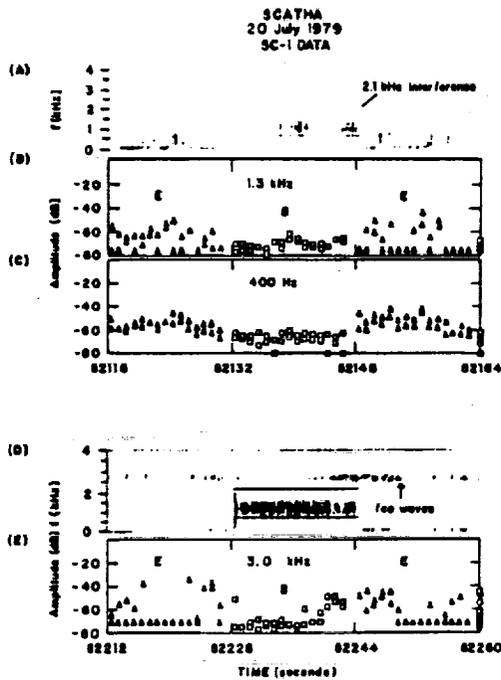
Figure 10.   SCATHA plasma wave data for electron gun off conditions. The wideband receiver was in its 0–3 kHz mode. Selected channels of the narrowband receiver are plotted below the wideband data.
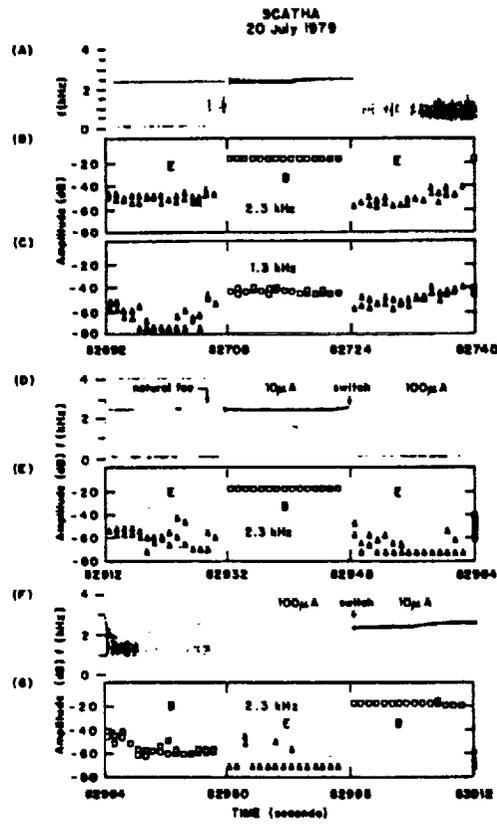
Figure 11.   SCATHA plasma wave data for electron gun on conditions.
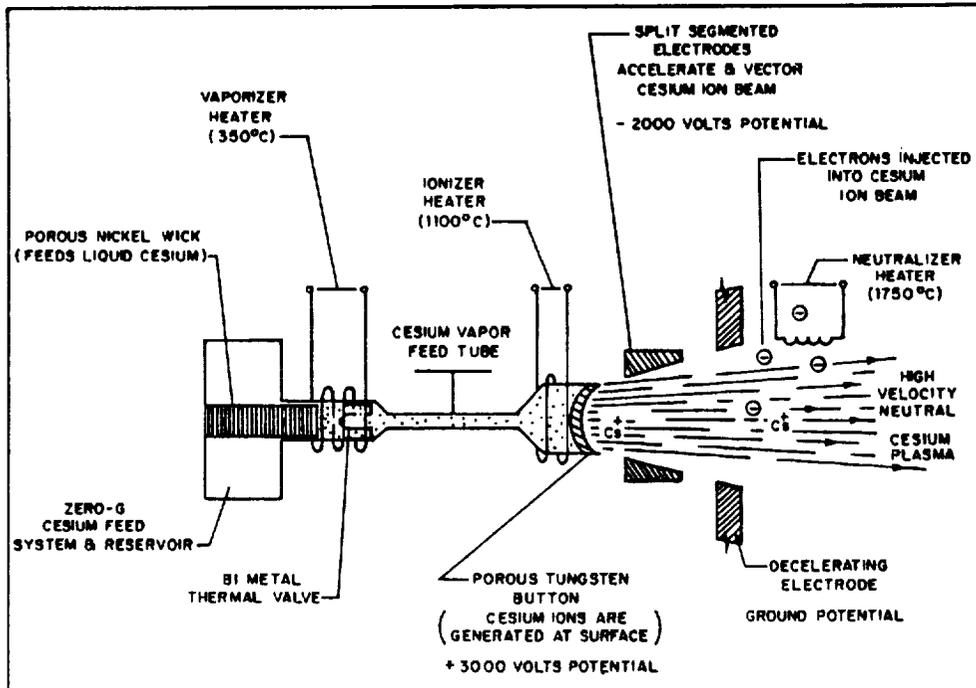
Figure 12.   ATS–5 Ion thruster.
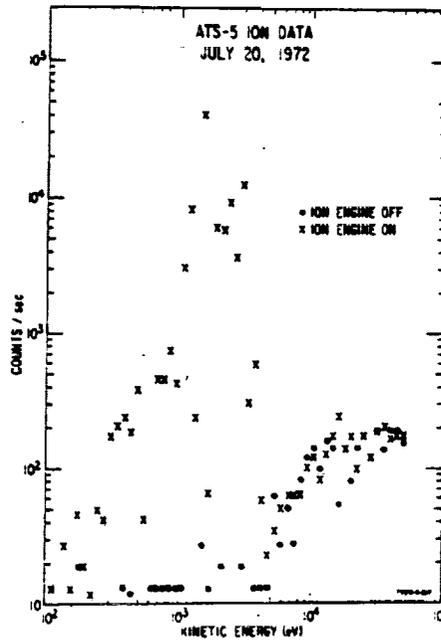
Figure 13.   ATS–5 ion flux for ion thruster non–neutral beam experiments. Two consecutive 20 second scans are plotted. When the engine is on, there is a peak in the flux from 1–3 keV indicating a negative potential of –1 to –3 kV. The spacecraft potential is presumably varying on a time scale which is comparable to the energy step period (~ 0.23 seconds).

Spacecraft potential as a function of neutralizer bias voltage. Ion beam current, 253 milliamperes.
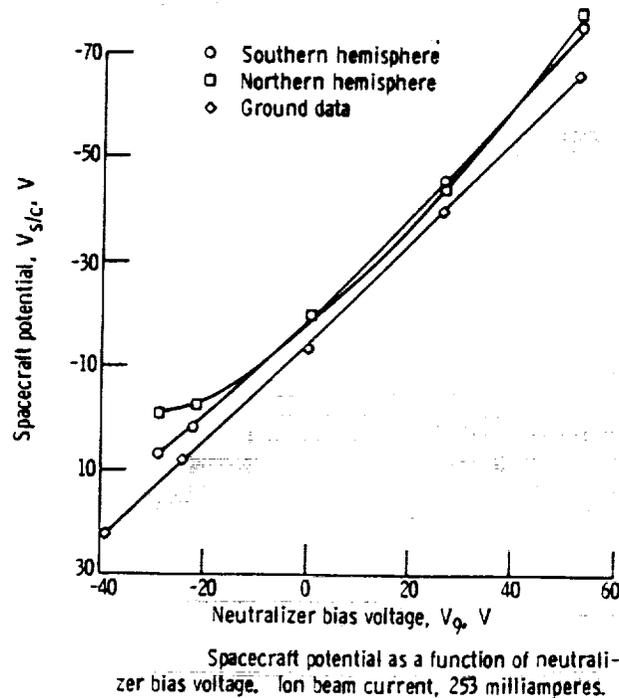
Figure 14.   SERT II spacecraft potential measurements during neutralizer bias experiments. Ion beam current is 253 mA [Jones et al, 1970].
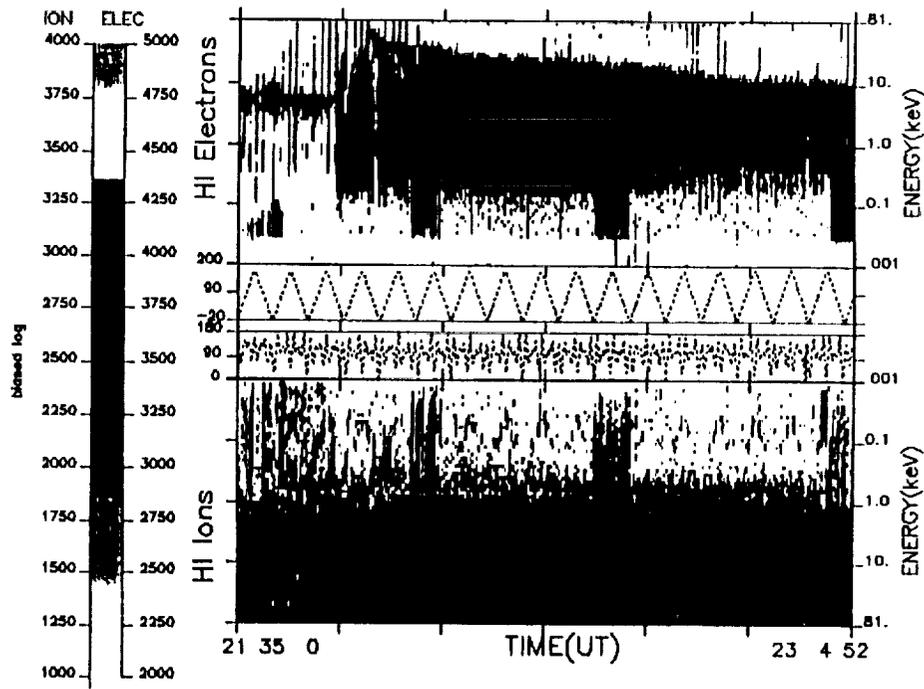
Figure 15.   SCATHA electrostatic analyzer data for ion gun experiments on 19 July 1979. The gun is operated at 1 kV, ~ 1 mA.
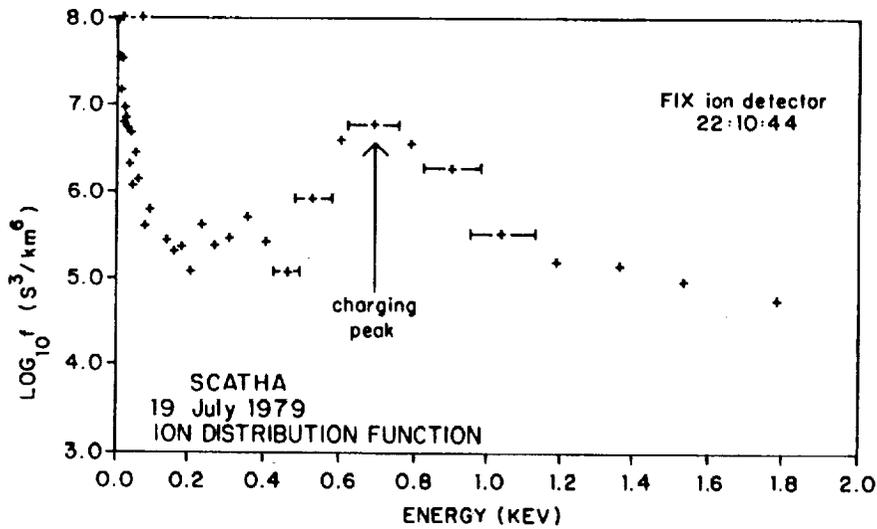
Figure 16.   SCATHA ion distribution function, 19 July 1979.
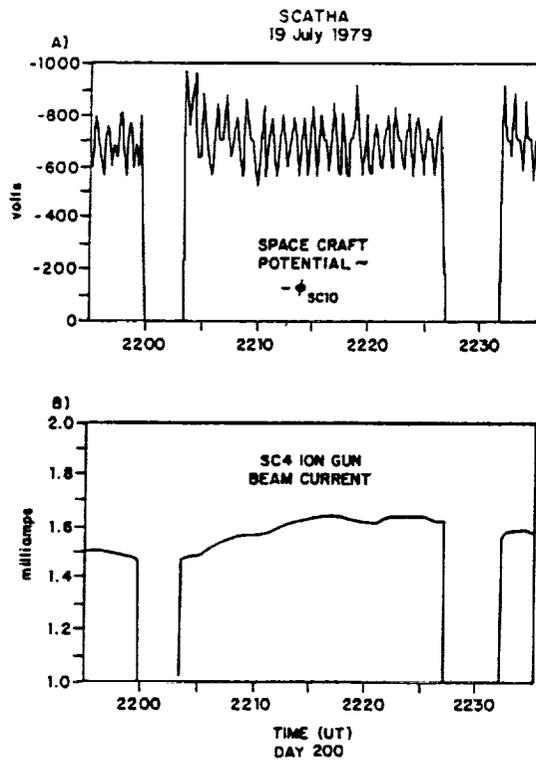
Figure 17.   a.   Spacecraft potential estimate using the SC10 electric field data. the floating potential of one 50–m antenna segment is plotted.

              b.   Ion gun beam current for 19 July 1979 (Day 200).
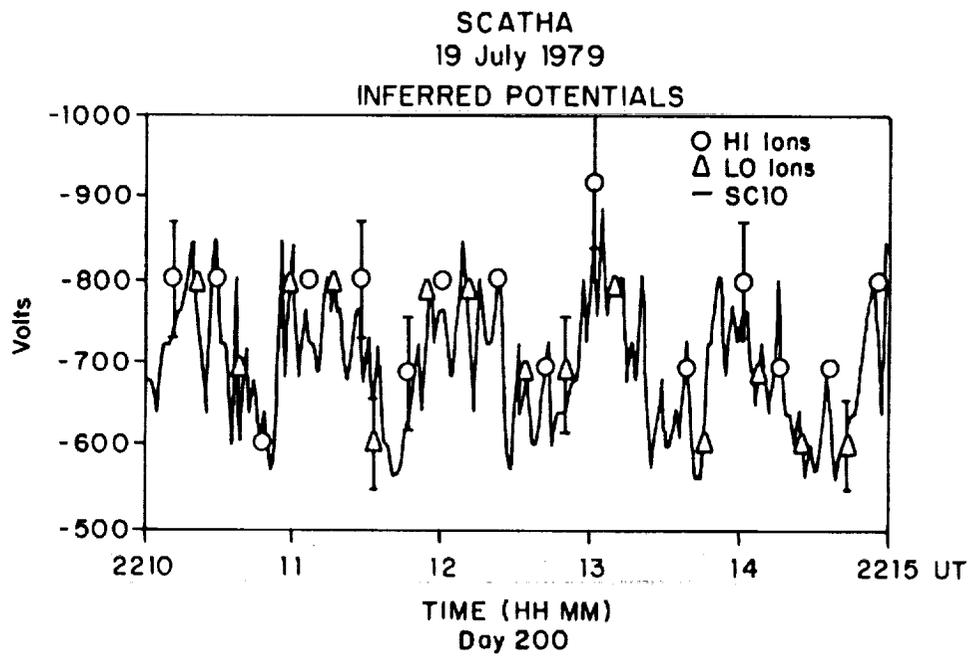
Figure 18.   SCATHA SC10 and SC9 potential measurements for a subset of the period shown in Figure 17.

SCATHA
19 July 1979
ION DISTRIBUTION FUNCTION
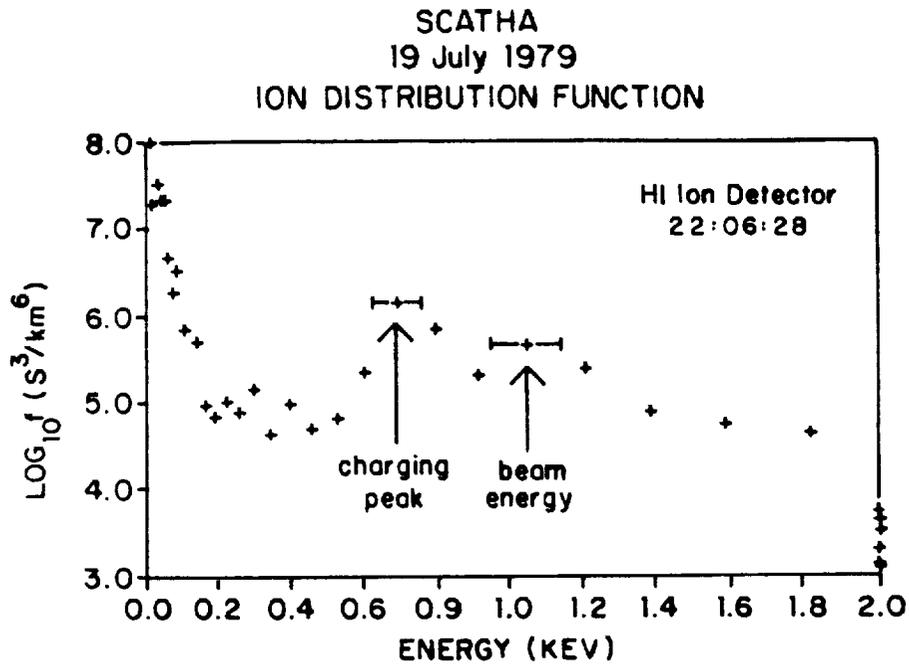
Figure 19.   SCATHA ion distribution function, as in Figure 16. There are two relative maxima. The spacecraft potential is associated with the 700 eV peak, returning beam ions with the 1 keV peak.
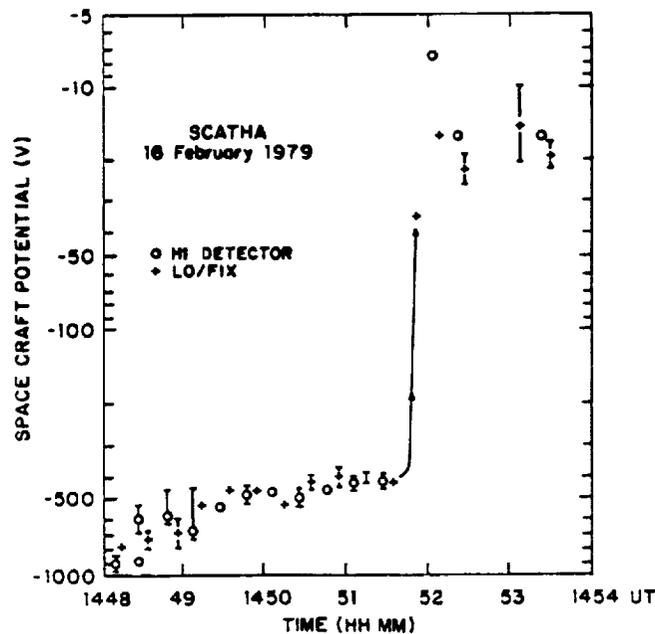
Figure 20.   SCATHA potentials, for ion gun operation on 16 February 1979 (Day 47), inferred from the peak in the electrostatic analyzer ion data.

Space Charge Limiting—Ions
Virtual Anode Effect
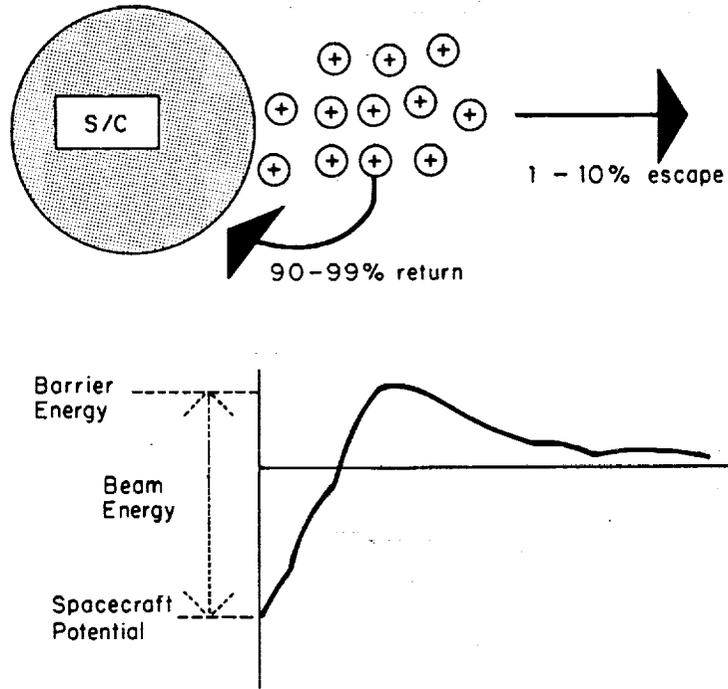
Figure 21.   Cartoon illustration of the virtual anode effect in current limiting the ion beam.